1 Theory

1.1 Dislocation lines

Several investigations have documented that dislocations in silicon give rise to characteristic photoluminescence (PL) spectra below the band edge. First showed in [1] which labeled them D1 (0.812eV), D2 (0.875eV), D3 (0.934eV) and D4 (1.000eV). The samples where deformed at 850° C by bending, so that dislocation densities was inhomogeneous along the samples. [1] states that the intensity of theese lines increase closer to the dislocation-rich parts of the crystal. At the same time the intensity of the intrinsic characteristics decrease. The distance between D1-D4 (62 ± 3 meV) corresponds to the energy of the optical phonons in silicon [1]. [1] reports that D1 and D2 are dominant in heavily deformed Si crystals, while D3 and D4 predominate in weakly deformed Si. A similar result was also reported by recent study [2] for small angle grain boundaries using cathodoluminescence.

It has been suggested in [3] that D1-D4 are due to dislocations which have been frozen in under low-shear stress. [3] state that photoluminescence under uniaxial stress shows that D1/D2 originate in the tetragonal defect with random orientation relative to <100> directions. [3] conclude that D3 and D4 are closely related, whereas the independent D1/D2 centers might be deformation-produced point defects in the strain region of dislocations. D1 and D2 is known to be closely related, as well as D3 and D4, and there have been no reports on the D-line spectrum missing only the D1 line [4].

The origin of D1 and D2 is not clear. It has been argued that they originate in electronic transition at the geometrical kinks on dislocations [5], point defects [3] and impurities [6] and/or from the reaction products of dislocations [7]. On the other hand, D3 and D4 lines is generally thought to be related to electronic transition within dislocation cores [8]. In addition, it has been suggested that the D3 line most likely is a phonon-assisted replica of D4 [8].

New lines D5 and D6 emerge when high-temperature, low-stress deformation is followed by low-temperature, high-stress deformation. [3] propose that line D5 is due to straight dislocations and D6 is due to stacking faults. [3] also suggest that D3/D4 photoluminescence is much more characteristic of the dislocations themselves than the D1/D2 emission lines. [9] state that D5 is correlated with electron-hole recombination at localized centers on separate partial dislocations. After annealing at moderate temperatures (T > 360°C) the new lines merge into D4 [9].

Both [1] and [3] studied plastically deformed silicon made by the Czochralski process (Cz-Si). [10] studied dislocations in multicrystalline silicon (mc-

Si) and found similar lines with the entire set of D-lines shifted with around 10meV, presumably due to a strain field. Using a laser annealing technique [11], introducing dislocations on a Cz-Si wafer, confirm the band location of D1-D4 from [3] in [10]. A principal difference between dislocation D'-lines in mc-Si versus D-lines in Cz-Si is a substantial broadening (60-70meV at 77K) of the D1'/D2' lines [10].

Cz-Si [1]	D1	D2	D3	D4
	0.812eV	0.875eV	0.934eV	1.000eV
mc-Si [10]	D1'	D2'	D3'	D4'
	0.80eV	0.89eV	0.95eV	1.00eV

Table 1: Energy positions of dislocation D-lines in Cz-Si and D' bands in mc-Si

[10] reveal a linear dependence of the band-to-band photoluminescence intensity and minority carrier lifetime across entire multicrystalline-Si wafers. Photoluminescence mapping in [10] of the 0.78eV (0.8eV) band intensity reveal a linkage to areas of a high dislocation density. This band should also be visible in room temperature [10].

Dislocation related lines (D-lines) has been observed in low temperature photoluminescence spectra from the regions which included the intragrain defects. [4] concluded that grain boundaries are not active recombination centers. [4] also show a TO-phonon replica of the boron bound exiton at 1.093eV. Intensity of boron bound exciton from the long lifetime regions was higher than that from the short lifetime regions. D-lines reported by [3] are in a short lifetime region. For a long lifetime region, [4] observe a peak at 1.00eV which is not the D4 line, but the zone center optical phonon sideband of the two-hole transition in the boron bound exiton [12].

It is believed that the intra-grain defects observed in the photoluminescence mapping are dislocations decorated with the heavy metals [4]. [13] found that if the contamination level is too low, or too high (dislocation decorated by metal silicate precipitates) the defect photoluminescence band vanished in room temperature. However, a relatively low contamination level of dislocations, in the order of 10 impurity atoms per micron of the dislocation length produces distinguishable defect band luminescence [13].

[14] conclude that defects are metal contaminated dislocation clusters which originated from small angle grain boundaries. [14] study origins of the defects by low temperature photoluminescence spectroscopy, electron backscatter diffraction pattern measurement and the etch-pit observation. [15] demonstrate three areas of a sample with only D3 and D4 present, and

conclude that this is due low concentration of metallic impurities.

1.2 Impurities

Diffusion of transition metals into silicon crystals result in a variety of different electrically active levels in the forbidden bandgap. Impurities is also known to create precipitates inside a silicon crystal, which change the photoluminescence spectra compared to interstitial impurities.

There are several units of impurities in silicon that's commonly used. Examples are: ppbw (Parts Per Billion by Weight), ppba (Parts per Billion Atomic) and atoms/cm^3. To convert from ppbw to atoms/cm^3, the following equation can be used:

$$atoms/cm^{-3} = 10^{-9}[ppbw] \cdot N_A \cdot [density(Si)]/[atomicmassofelement] \quad (1)$$

where N_A is Avogradro's number, density(Si) is in g/cm^3, and atomic mass is in g/mol. To convert from ppba to ppbw:

$$ppbw = [atomicmassofelement]/[atomicmassofSi] \quad (2)$$

1.2.1 Atom impurities

Early work done by [12] compare intrinsic silicon from the Czochralski process with doped silicon. [12] do extensive photoluminescence study with doping atoms As, P, Sb, Bi, B, Ga, In and Al. The high intensity transverse optical lines occur at 1.0907eV, 1.0916eV, 1.0921eV, 1.0888eV, 1.0924eV, 1.0914eV, 1.0835eV and 1.092eV respectively with the different doping atoms present. Impurities like carbon complexes with many impurities in silicon, resulting in a large variety of photoluminescence centers. Detected complexes are another C atom, one oxygen atom, one N atom, one Ga atom, the four-lithium atom complex, beryllium and numerous radiation damage centres, especially involving oxygen [16]. See appendix 5 for energies.

Doping atoms give rise to different characteristics in the photoluminescence spectra aswell. Boron doping exhibits a line right below the silicon bandgap. That particular peak is hard to detect due to a strong luminescence from the silicon itself, but its phonon replicas can be identified (figure 4). Phosphorous doping give rise to a line just below the boron line (figure 5).

Some impurities does not result in any specific photoluminescence spectra, like interstitial chromium [17]. Atleast not for wavelengths up to 1800nm. However, chromium bound with a boron atom can be identified as a peak

around 0.85eV where the intensity increase linearly with laser power [17, 18]. Photoluminescence from another impurity, titanium, has been observed around 2.85eV in 4H silicon carbide by [19], and in 6H by [20] at 2.79eV, 2.82eV and 2.86eV named ABC lines (figure 9). These energies are far beyond that of the silicon bandgap, and can in cases described above, be uniquely identified.

Many of the other identified impurities are located just below the silicon bandgap in the photoluminescence spectra. Spectra for a silicon sample with a low amount of impurities can be seen in figure 3. Copper doping of silicon crystals results in an intense emission at 1.014eV [21]. [9] study Cu doped Si and also observe a shoulder on the D1 line which presumably arises from Cu precipitates at the dislocation.

Another important impurity is iron. [22] observe a spectrum of 0.735eV, which relate to a complex defect containing iron. Here the sample was introduced with Fe atoms into a float-zone silicon crystal (PL at figure 6). An earlier study [23], observe a luminescence spectra around 1.07eV in boron-doped, iron-diffused crystalline silicon and suggest the source is Fe-B pairs. Interstitial iron Fe, is about 10 times more effective as a recombination center than Fe-B pairs by low-level lifetime measurements and therefore reduces the minority carrier diffusion length more strongly (PL at figure 7) [24].

Recent work in [25] show that micro-photoluminescence is an excellent tool for identifying metal precipitates in silicon as seen in figure 1. Iron images in [26] reveal internal gettering of iron to grain boundaries and dislocated regions during ingot growth. The minimum size for detection is 1μm, or even smaller, since the photoluminescence signal might be broadened. Precipitates from Fe and Cu are detected due to reduced band to band recombination intensity. Iron in silicon also affect the defect photoluminescence [25].

1.2.2 Interaction with dislocations

Investigation in [27] show that transition-metal contamination plays an important role in the production of D-band luminescence from silicon samples containing either epitaxial stacking faults or oxidation-induced stacking faults. [11] found that Cu doping resulted in reduced intensity of D1 and D2, and the intensity of D3 and D4 become very small. [9] demonstrate that a complete passivation of the D-band luminescence is achieved at higher Cu and Fe concentration when deliberately contaminating high purity silicon samples which contain dislocations. However impurities like Ni, lead to no detectable changes in the spectrum [9]. D-band recombination in Si is found to be independent of impurities trapped at dislocations [9], and [7] concluded

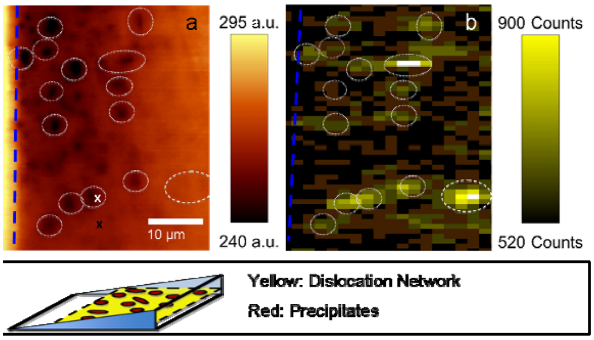

Figure 1: Bottom: Scheme of the sample preparation with the polished angle. Top: A Intensity of the BB PL peak at room temperature (a), and of the iron X-ray Kα fluorecence (b) from [25]. The dislocation network intersects the surface to the right of the dashed blue line. The white circles show recombination active precipitates.

that metallic impurities don't seem to be related to D1 and D2 luminescence. Even so, it is still generally accepted that metal impurity influence it. Metal precipitation at crystal defects during the crystal growth can clean grains from impurities, and thus improve the performance as suggested for iron in [28]. A recent example of interaction with defects is iron precipitates in [25], showing an enhanced defect photoluminescence at 1.3μm (0.95eV). The same study show that copper contamination almost completely suppress the defect photoluminescence. This is in agreement with [11]. Supression of defect photoluminescence by high copper concentrations was also reported in [29]. Cu precipitates can be located by reduced intensity of the band to band photoluminescence peak, both in areas with dislocations, and without [25].

Electron hole droplets (EHD), free excitons (FE) and bound excitons (BE) localized on phosphorus atoms has been steadily observed in [30] with photoluminescence on samples with low-dislocated regions. When increasing dislocation density the FE, BE and EHD bands decrease sharply. This may be due exciton capture by dislocation lines D1,D2 and non-radiative recombination [30]. EHD photoluminescence intensity is highly dependent on the pumping power [31]. There is a linear dependence, and pumping with 3mW or less makes it hardly visible in [31].

D1 line is shifted towards higher energies under uniaxial elastic deformation of samples with introduced dislocations or after their annealing in oxygen at 750°C [32]. Room temperature mapping of the 0.77eV band is attributed to oxygen precipitates in in thermally treated silicon made by the Czochralski process (Cz-Si) [33]. The increase of this band on the dislocation

lines is due to the preferential precipitation of oxygen [33]. Later, [34] state that the deep-level emission from multicrystalline silicon with an intensity maximum at 0.78eV at room temperature is different from that of the D1 line at low temperature. Furthermore, [34] suggest that the 0.78eV emission is associated with oxygen precipitation, and that the intra-grain defects are dislocation clusters decorated with oxygen impurities in addition to heavy-metal impurities. [35] state that the origin of trap densities in multicrystalline silicon could be structural crystal defects, which are highly decorated with oxygen precipitates.

2 Experimental

2.1 Samples

Name	Description	Quality	Feedst
R6-Q3-210	Polysilicon, good quality	Electronic grade	Feedstock from Si
ES1-Q3-201	Large amount of P and B	Solar grade	Feedstock from
MH2-Q3-201	Large amount of P and B, and added Cr	Solar grade	Feedstock from

Table 2: Samples of interest

2.1.1 R6-Q3-201

This sample is from a clean feedstock, with low amount of impurities. B,Al and Fe where measured by Glow-Discharge Mass Spectrometry (GDMS), O and C where measured by Fourier transform infrared spectroscopy (FTIR).

Impurity	ppbw	atoms/cm^3
B	112.01	$1.45 \cdot 10^{16}$
Al	19.48	$1.0 \cdot 1010^{15}$
Fe	nd	nd
C	2576	$2.26 \cdot 10^{17}$
O	1932	$8.87 \cdot 10^{16}$

Table 3: Impurities in R6

The impurities that are not listed were not analyzed, and are expected to be present in very low levels (tenths of ppbs).

2.1.2 ES1-Q3-201

This is a regular solar grade sample which originate from a compensated feedstock from Elkem Solar, from 90% ingot height. It has been Sopori etched to bring out dislocations [37].

Boron contaminants appear to be between 550 and 700 ppbw, which is between 7.1 $\cdot 10^{16}$ and 9.7 $\cdot 10^{16}$ atoms/cm^3 respectively using 1. Phosphorus is measured around 1200-1500 ppbw, which is 5.4-6.8 $\cdot 10^{16}$ atoms/cm^3. Aluminum contaminants is just below 2.6*10^{15} atoms/cm^3. Other contaminants like Ti and Fe have very low values: less than 1.2 $\cdot 10^{14}$ and 3.8 $\cdot 10^{14}$ atoms/cm^3 respectively. For the lighter atom impurities, O have $1.7 * 10^{17}$ atoms/cm^3 and C have $6 * 10^{17}$ atoms/cm^3 [36].

2.1.3 MH2-Q3-201

This sample is almost identical to ES1, but the sample also have extra chromium added. Chromium contaminants appear to be between 2 and 5 ppbw [36] which corresponds to $5.4 \cdot 10^{13}$ and $1.3 \cdot 10^{14}$ atoms/cm^3 respectively using 1, but exact concentration might be a little lower due detection limit of the instrument.

2.2 Setup

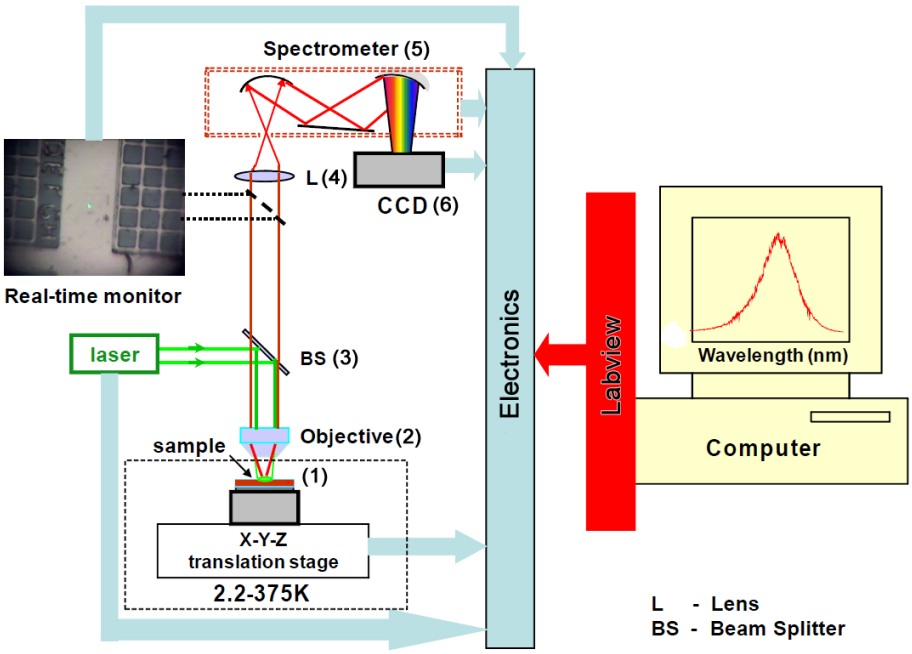

Figure 2: Lab setup

#	Part	Product #	Manufacturer
1	Cryostat	Janis ST-500	Janis Research Company
2	Objective	NT56-982	Edmund Optics
3	Beam splitter	BS017	Thorlabs
4	Lens	ACN127-020-B	Thorlabs
5	Spectrometer	iHR550 Imaging Spectrometer	Horiba Scientific
9	Camera	InGaAs Spectroscopy CCD	Andor Technology

Table 4: Lab setup optical components

2.3 Pumping wavelength

Pumping light needs to have enough energy to fill all available states in the crystal lattice, in order to detect defects and impurities. For silicon, which has a bandgap of around 1.1eV, has most impurity/defect bands below the bandgap. In order to fill these states, the pumping wavelength should be below 1125nm, which corresponds to energies just over 1.1eV.

Silicon has different absorption lengths for different wavelengths. For 1125nm, the absorption depth is nearly 200 μm [38]. Compared to absorption for 532nm, 1125nm reach 200 times deeper into the sample.

Absorption length of about 1 μm for 532 nm laser, means that iron precipitates deeper in the sample won't be detected [25]. This limitation might be overcome by an excitation laser with a longer wavelength and absorption length in silicon. [2] report that small angle grain boundaries in multicrystalline silicon of 1°-1.5° show D3 and D4 lines, while 2°-2.5° show D1 and D2 lines. Comparing to data from electron beam induced current measurements show D1 and D2 lines to be correlated with shallow levels, while D3 and D4 appear in both shallow and deep levels [2].

A pumping wavelength of 800 nm is chosen for excitation. This corresponds to an absorption depth of 12 μm in silicon. With a larger wavelength, it would be invisible to the naked eye, and make it much more difficult to align the setup, and make sure nothing is blocking the pathway. In the case of an imperfect filter in front of the spectrometer, 800nm (1.55eV) and the second order diffraction maxima at 1600 nm (0.775 eV) would be outside the most interesting wavelengths from silicon luminescence (see table 5).

2.4 Spot size

Having a small diameter on the pumping laser allows for a high resolution of characteristics on the sample. In an iron contaminated sample, [25] show that at some distinct spots of a size between 1μm and 4μm, the band to band photoluminescence peak is particular low at spots with iron precipitates.

A large electron hole droplet could overshadow characteristics from impurities in the sample. [31] show that electron hole droplets become more intense for a smaller volume, with a silicon nanolayer smaller than the absorption depth of the laser. [31] used a 488nm pumping laser with 1,5μm diameter, on silicon nanolayer thickness of 50nm and 340nm. For the 50nm layer, [31] observed a large electron hole droplet, even for small pumping intensities, with the same amount of photo excited carriers per volume as for the 340nm layer. Assuming that a small volume give rise to a larger electron hole droplet, it would be a limiting factor for the spot size and pumping

wavelength.

For the setup given here, the spot size is around 2 μm.

2.5 Laser intensity

With a large pumping intensity, an electron hole droplet become visible in the specter around 1.08eV in bulk silicon [39]. [31] show that electron hole droplets occur at weak excitations (0.75mW) and even at high temperatures for a silicon nanolayer of 50nm. For thickness of 340nm, the electron hole droplet show up at pumping intensity of 3mW and above, and the intensity of the electron hole droplet grow larger than for the free exciton at 15mW. This electron hole droplet is not wanted, as it can mask characteristic photoluminescence from impurities.

With a larger pumping intensity, the impurity photoluminescence would in some cases also increase. Photoluminescence from chromium bound with a boron atom is known to increase linearly with laser power [17, 18], and would be easier to detect at a higher pumping intensity.

2.6 Expected results

2.6.1 Phosphorus and boron doped samples

With fairly high concentrations of doping atoms, it's expected that they show up as separate lines in the photoluminescence spectra. [12] observe a line around 1.0924eV which is attributed to B^{TO}. Concentrations values for B in [12] are $6 * 10^{16}$ cm^{-3}. Also observed is a phosphorus line at 1.0916eV, with 8*10^{16}cm$^-$3 phosphorus atoms. ES1 and MH2 have similar B and P values, and is expected to show the same behavior.

2.6.2 Chromium contaminated sample

The closest comparison is samples used in [17]. Here, luminescence spectra was observed for chromium in an p-type sample. Interstitial chromium concentrations where between 10^14 and $10^16 atoms/cm^-3$ in [17],

Chromium in an n-type sample does not result in any luminescence, but chromium bound with boron show a clear line at 0.8432eV (CrB^0). The reaction velocity for the formation of CrB pairs at room temperature depend on the boron concentration. For large (10^15cm$^-$3) boron content, the chromium-boron reaction reach saturation in less than a day after chromium diffusion [17].

References

[1] N. A. Drozdov, A. Patrin, and V. Tkachev, "Recombination radiation on dislocations in silicon," *Pis'ma Xh. Eksp. Teor. Fiz.*, 1976.

[2] W. Lee, J. Chen, B. Chen, J. Chang, and T. Sekiguchi, "Cathodoluminescence study of dislocation-related luminescence from small-angle grain boundaries in multicrystalline silicon," *Applied Physics Letters*, 2009.

[3] R. Sauer, J. Weber, and J. Stolz, "Dislocation-related photoluminescence in silicon," *Appl. Phys.*, 1985.

[4] H. Sugimoto, M. Inoue, M. Tajima, A. Ogura, and Y. Ohsita, "Analysis of intra-grain defects in multicrystalline silicon wafers by photoluminescence mapping and spectroscopy," *Japanese Journal of Applied Physics*, 2006.

[5] M. Suezawa, Y. Sasaki, and K. Sumino, "Dependence of photoluminescence on temperature in dislocated silicon crystals," *Physica Status Solidi*, 1983.

[6] V. Higgs, P. Kightley, P. Goodhew, and P. Augustus, "Metal-induced dislocation nucleation for metastable sige/si," *Appl. Phys. Lett.*, 1991.

[7] T. Sekiguchi and K. Sumino, "Cathodoluminescence study on dislocations in silicon," *J. Appl. Phys.*, 1995.

[8] V. Kveder, E. Steinman, S. Shevchenko, and H. Grimmeiss, "Dislocation-related electroluminescence at room temperature in plastically deformed silicon," *Phys. Rev. B*, 1995.

[9] K. Weronek, J. Weber, and R. Buchner, "Origin of d-band photoluminescence in silicon," *Springer Proceedings in Physics*, 1991.

[10] I. Tarasov, S. Ostapenko, C.Haessler, and E.-U. Reisner, "Spatially resolved defect diagnostics in multicrystalline silicon for solar cells," *Elsevier Science S.A*, 2000.

[11] W. Staiger, G. Pfeiffer, K. Weronek, A. Höpner, and J. Weber, "Dislocation-induced defect levels in silicon," *Materials Science Forum*, 1994.

[12] P. J. Dean, J. Haynes, and W. Flood, "New radiative recombination processes involving neutral donors and acceptors in silicon and germanium," *Physical Review Volume 161 Number 3*, 1967.

[13] I. Tarasov, S. Ostapenko, W. Seifert, M. Kittler, and J. Kaleis, "Defect diagnostics in multicrystalline silicon using scanning techniques," *Elsevier Science B.V.*, 2001.

[14] H. Sugimoto, K. Araki, M. Tajima, T. Eguchi, I. Yamaga, M. Dhamrin, K. Kamisako, and T. Saitoh, "Photoluminescence analysis of intragrain defects in multicrystalline silicon wafers for solar cells," *Journal of Applied Physics*, 2007.

[15] T. V. Arguirov, "Electro-optical properties of dislocations in silicon and their possible application for light emmiters," ., 2007.

[16] G. Davies, "The optical properties of luminescence centres in silicon," *Physics Report*, 1988.

[17] H. Conzelmann, K. Graff, and E. Weber, "Chromium and chromium-boron pairs in silicon," *Appl. Phys. A*, 1982.

[18] H. Conzelmann and J. Weber, "Photoluminescence from chromium-boron pairs in silicon," *Physica*, 1983.

[19] L. Patrick and W. Choyke, "Photoluminescence of ti in four sic polytypes," *Physical Review B*, 1974.

[20] A. van Kemenade and S. Hagen, "Proof of the involvement of ti in the low-temperature abc luminescence spectrum of 6h sic," *Solid State Communications*, 1974.

[21] J. Weber, H. Bauch, and R. Sauer, "Optical properties of copper in silicon: Excitons bound to isoelectronic copper pairs," *Physical Review B*, 1982.

[22] M. Càlão and M. do Carmo, "Luminescence from an iron related deep center in silicon," *Physica Scripta*, 1988.

[23] H. Mohring, J. Weber, and R. Sauer, "Photoluminescence of excitons bound to an isoelectronic trap in silicon associated with boron and iron," *Physical Review B*, 1983.

[24] G. Zoth and W. Bergholz, "A fast preparation-free method to detect iron in silicon," *J. Appl. Phys*, 1990.

[25] P. Gundel, M. C. Schubert, W. Kwapil, J. Schön, M. Reiche, H. Savin, M. Yli-Koski, J. A. S. ans Gema Martinez-Criado, W. Seifert, W. Warta, and E. R. Weber, "Micro-photoluminescence spectroscopy on metal precipitates in silicon," *Phys. Status Solidi RRL*, 2009.

[26] D. Macdonald, J. Tan, and T. Trupke, "Imaging interstitial iron concentrations in boron-doped crystalline silicon," *Journal of applied physics*, 2008.

[27] V. Higgs, M. Goulding, and P. Kightley, "Characterization of epitaxial and oxidation-induced stacking faults in silicon: The influence of transition-metal contamination," *Appl. Phys. Lett.*, 1992.

[28] J. Bailey and E. R. Weber, "Precipitation of iron in polycrystalline silicon," *Physica Status Solidi (a)*, 1993.

[29] E. C. Lightowlers and V. Higgs, "Luminescence associated with the presence of dislocations in silicon," *Physica Status Solidi (a)*, 1993.

[30] N. Drozdov and A. Fedotov, "Electron-hole drops in dislocational silicon," *Microelectronic Engineering 66*, 2002.

[31] S. Nihonyanagi and Y. Kanemitsu, "Enhanced luminescence from electron-hole droplets in silicon nanolayers," *Applied physics letters*, 2004.

[32] N. A. Drozdov, A. A. Patrin, and V. T. Tkachev, "Modification of the dislocation luminescence spectrum by oxygen atmospheres in silicon," *physica status solidi (a)*, 1981.

[33] M. Tajima, M. Tokita, and M. Warashina, "Photoluminescence due to oxygen precipitates distinguished from the d-lines in annealed si," *Materials Science Forum*, 1995.

[34] M. Inoue, H. Sugimoto, M. Tajima, Y. Ohshita, and A. Ogura, "Microscopic and spectroscopic mapping of dislocation-related photoluminescence in multicrystalline silicon wafers," *J. Mater Sci*, 2007.

[35] P. Gundel, M. C. Shubert, and W. Warta, "Origin of trapping in multicrystalline silicon," *Journal of applied physics*, 2008.

[36] M. Hystad, "The distribution and impact of chromium impurities in compensated sog-silicon," Master's thesis, The Norwegian University of Science and Technology, 2009.

[37] B. Sopori, "A new defect etch for polycrystalline silicon," *J. Electrochem. Soc.*, 1984.

[38] E. Palik., *Handbook of optical constants of solids*. 2001.

[39] R. Hammond, T. McGill, and J. Mayer, "Temperature dependence of the electron-hole-liquid luminescence in si," *Physical Review B*, 1975.

[40] B. G. Streetman and S. K. Banerjee, *Solid state electronic devices*. Prentice Hall, 2006.

[41] T. Arguirov, W. Seifert, and M. K. J. Reif, "Temperature behaviour of photoluminescence and electron-beam-induced current recombination behaviour of extended defects in solar grade silicon," *J. Phys: Condens*, 2002.

[42] R. Sauer, J. Weber, , and J. Stolz, "Dislocation-related photoluminescence in silicon," *Applied Physics*, 1985.

[43] V. V. Kveder, E. A. Steinman, S. A. Shevchenko, and H. G. Grimmeiss, "Dislocation-related electroluminescence at room temperature in plastically deformed silicon," *Phys. Rev. B*, 1995.

[44] K. Leosson, J. Jensen, J. Hvam, and W. Langbein, "Linewidth statistics of single ingaas quantum dot photoluminescence lines," 2000.

[45] T. Arguirov, W.Seifer, G. Jia, and M. Kittler, "Photoluminiscence study on defects multicrystalline silicon," *Semiconductors*, 2006.

[46] A. J. Kenyon, C. E. Chryssoua, C. W. Pitta, T. Shimizu-Iwayamab, D. E. Holec, N. Sharmad, and C. J. Humphreysd, "Broad-band and flash-lamp pumping of 1.53 μm emission from erbium-doped silicon nanocrystals," 2001.

[47] B. Jalali, "Physics and technology forefronts - silicon lasers," *American Physical Society*, 2006.

[48] M. Inoue, H. Sugimoto, M. Tajima, Y. Ohshita, and A. Ogura, "Microscopic and spectroscopic mapping of dislocation-related photoluminescence in multicrystalline silicon wafers," *Mater Electron*, 2008.

[49] E. Katz, M. Koltun, and L. Polyak, "Polycrystalline silicon solar cells: Improvements in efficiency through hydrogen passivation," *Diffusion and Defect Data Pt.B: Solid State Phenomena*, 1996.

[50] T. Arguirov, W. Seifert, M. Kittler, and J. Reif, "Temperature behaviour of extended defects in solar grade silicon investigated by photoluminescence and ebic," *Elsevier B.V.*, 2003.

[51] S. Binetti, J. Libal, M. Acciarri, M. D. Sabatino, H. Nordmark, E. Øverlid, J. Walmsley, and R. Holmestad, "Study of defects and impurities in multicrystalline silicon grown from metallurgical silicon feedstock," *Materials Science and Egnineering B*, 2008.

[52] L. Patrick and W. Choyke, "Photoluminescence of ti in four sic polytypes," *Physical Review B*, 1974.

[53] M. Wagner, I. Ivanov, L. Storasta, J. Bergman, B. Magnusson, W. Chen, and E. Janzén, "Photoluminescence upconversion in 4h-sic," *Applied Physics Letters*, 2002.

[54] B. Sopori, P. Rupnowski, V. Mehta, V. Budhraja, S. Johnston, N. Call, H. Moutinho, M. Al-Jassim, A. Shaikh, M. Seacrist, and D. Carlson, "Performance limitations of mc-si solar cells caused by defect clusters," *Conference Paper NREL/CP-520-45012*, 2009.

[55] J. Dean, "Photoluminescence as a diagnostic of semiconductors," *Prog. Crystal growth charact.*, 1982.

[56] H. Conzelmann, "Photoluminescence of transition metal complexes in silicon," *Appl. Phys. A*, 1987.

[57] M. Kittler, W. Seifert, T. Arguirov, I. Tarasov, and S. Ostapenko, "Room-temperature luminescence andelectronbeam-induced current (ebic) recombination behaviour of crystal defects in multicrystalline silicon," *Solar Energy Materials and Solar Cells*, 2002.

[58] S. A. Shevchenko and A. N. Izotov, "Dislocation-induced photoluminescence in silicon crystals of various impurity composition," *Physics of the Solid State*, 2003.

[59] T. Trupke, R. A. Bardos, M. C. Schubert, and W. Warta, "Photoluminescence imaging of silicon wafers," *Applied Physics Letters*, 2006.

[60] J. Bauer, O. Breitenstein, and J.-P. Rakotoniaina, "Electronic activity of sic precipitates in multicrystalline solar silicon," *phys. stat. sol. (a)*, 2007.

[61] V. Karasuyk, A. Steele, A. Mainwood, E. Lightowlers, and G. Davies, "Ultrahigh-resolution photoluminescence studies of excitons bound to boron in silicon under uniaxial stress," *Physical Review B*, 1992.

[62] M. Kasemann, D. Grote, B. Walter, W. Kwapil, T. Trupke, Y. Augarten, R. Bardos, E. Pink, M. Abbott, and W. Warta, "Luminescence imaging for the detection of shunts on silicon solar cells," *Prog. Photovolt: Res. Appl.*, 2008.

[63] M. Kasemann, W. Kwapil, B. Walter, J. Giesecke, B. Michl, M. The, J. Wagner, J. Bauer, A. Schütt, J. Carstensen, S. Kluska, F. Granek, H. Kampwerth, P. Gundel, M. Schubert, R. Bardos, H. Föll, H. Nagel, P. Würfel, T. Trupke, O. Breitenstein, M. Hermle, W. Warta, and S. Glunz, "Progress in silicon solar cell characterization with infrared imaging methods," *23rd European Photovoltaic Solar Energy Conference*, 2008.

[64] S. McHugo, H. Hieslmair, and E. Weber, "Gettering of metallic impurities in photovoltaic silicon," *Appl. Phys. A*, 1996.

[65] S. Ostapenko, I. Tarasov, J. Kalejs, C. Haessler, and E. Reisner, "Defect monitoring using scanning photoluminescence spectroscopy in multicrystalline silicon wafers," *Semicond. Sci. Technol.*, 2000.

[66] S. Pizzini, M. Acciarri, E. Leoni, and A. L. Donne, "About the d1 and d2 dislocation luminescence and its correlation with oxygen segregation," *phys. stat. sol. (b)*, 2000.

[67] E. Steinman, A. Kenyon, and A. Tereshchenko, "Time-resolved measurements of dislocation-related photoluminescence bands in silicon," *Semicond. Sci. Technol.*, 2008.

[68] H. Sugimoto, M. Tajima, T. Eguchi, I. Yamaga, and T. Saitoh, "Photoluminescence analysis of intra-grain defects in cast-grown polycrystalline silicon wafers," *Materials Science in Semiconductor Processing*, 2006.

[69] M. Tajima, "Characterization of semiconductors by photoluminescence mapping at room temperature," *Journal of Crystal Growth*, 1990.

A Silicon energy bands

Energy	Name	Temp.	Impurity / Defect	Observed in
0.735eV	ZPL	22K	Fe contamination	[22]
0.745eV	C-N		Carbon-Nitrogen complex	[16]
0.76-0.8eV	Defect	290K	Dislocation with low contamination	[10, 13, 45]
0.77-0.78eV	D_b	4.2-295K	Oxygen impurity band	[33, 34]
0.77eV	P line	12K	C-O complex related	[16, 51]
0.780eV	$CrB^{0\Gamma}$	4.2K	CrB^0 phonon replica	[18]
0.79eV	C-O	12K	Carbon-Oxygen complex	[16, 51]
0.80eV	D1'	77K	Dislocations [1]	[10, 13]
0.812eV	D1	4.2K	Dislocation related line [1]	[1, 3, 50]
0.8160	CrB^2	4.2K	Cr-B excitation of local vibrations	[18]
0.8402	CrB^1	4.2K	Cr-B excitation of local vibrations	[18]
0.8432eV	CrB^0	4.2K	Cr-B pair no-phonon	[17, 18]
0.875eV	C-Ga		Carbon-Gallium complex	[16]
0.875eV	D2	4.2K	Dislocation related line [1]	[1, 3, 50]
0.89eV	D2'	77K	Dislocations [1]	[10, 13]
0.8-0.9eV	D_{a1}	11K	Broad background emission under D1/D2	[33]
0.91eV	H-line	12K	C-O complex related	[16, 51]
0.93eV	H-line	12K	C-O complex related	[16, 51]
0.934eV	D3	4.2K	Dislocations [2]	[1, 3, 50]
0.95eV	D3'	77K	Dislocations [2]	[10, 13]
0.953eV	D5	4.2K	Straight dislocations	[3, 9]
0.9537eV	Defect	300K	Iron precipitate	[25]
0.968eV	I^{TO+20^Γ}	26K	TO + 2 Zone center phonon	[12]
0.969eV	C-C		Carbon-Carbon complex	[16]
0.98eV	R2BB	80K	Two phonon replica of band edge emission	[50]
0.9-1.0eV	D_{a2}	11K	Broad background emission under D3/D4	[33]
1.000eV	D4	4.2K	Dislocations [2]	[1, 3, 50]
1.00eV	D4'	77K	Dislocations [2]	[10, 13]
1.0089eV	FeB^0(TO)	6K	Fe-B pair phonon replica	[23]
1.0126eV	D6	4.2K	Stacking faults	[3, 9]
1.013eV	$I^{TO+0^\Gamma+IV^a}$	26K	$TO + 0^\Gamma + IV^a$ phonon	[12]
1.014eV	Cu_0	4.2K	Copper doping	[21, 9]
1.018eV	W/I1		Radiation damage	[16]
1.0315eV	I^{TO+0^Γ}	26K	TO + Zone center phonon	[12]
1.04eV	R1BB	80K	One phonon replica of band edge emission	[50]
1.045eV	Q		4-Li atom complex	[16]
1.0504eV	FeB^2	6K	Fe-B pair contamination	[23]

Continued on next page

Table 5 – continued from previous page

Energy	Name	Temp.	Impurity / Defect	Observed in
1.051eV	I^{TO+IV^b}	26K	Inter valley phonon replica	[12]
1.0595eV	FeB^1	6K	Fe-B pair contamination	[23]
1.0692eV	FeB^0	6K	Fe-B pair no phonon	[23]
1.074eV	I^{TO+IV^a}	26K	Inter valley phonon replica	[12]
1.078	EHD	4.2K	Electron Hole Droplet dislocation-area	[30]
1.082eV	EHD_{TO}	4.2K	Electron Hole Droplet dislocation-free	[39, 30, 31]
1.0835eV	In^{TO}	30K	Indium doping TO	[12]
1.0888eV	Bi^{TO}	15K	Bismuth doping TO	[12]
1.0902eV	Al^{TO}	30K	Aluminum doping TO	[12]
1.0907eV	As^{TO}	15K	Arsenic doping TO	[12]
1.0907eV	Ga^{TO}	15K	Gallium doping TO	[12]
1.0916eV	P^{TO}	15K	Phosphorus doping TO	[12]
1.092eV	BE1	4.2K	Bound exciton	[1]
1.0921eV	Sb^{TO}	15K	Antimony doping TO	[12]
1.0970eV	I^{TO}/FE	26K	Transversal Optical/Free exciton	[12, 39, 30]
1.0924eV	B^{TO}	15K	Boron doping TO	[12]
1.093eV	B_{TO}	4.2K	TO phonon replica of Boron bound exciton	[14, 34]
1.1365eV	I^{TA}/LO/FE	26K	Transversal Acoustic/Longitudinal/FE	[39, 12]
1.1545eV	I^0	26K	No phonon	[12]
2.786eV	$^4 8_C$Ti	4.2K	C line Ti isotope 48 impurity in 6H SiC	[20]
2.820eV	$^4 8_B$Ti	4.2K	B^0 line Ti isotope 48 impurity in 6H SiC	[20, 53]
2.85eV	^{4}8Ti	4.2K	Ti isotope 48 impurity in 4H SiC	[19]
2.861eV	$^4 8_A$Ti	4.2K	A^0 line Ti isotope 48 impurity in 6H SiC	[20, 53]

Table 5: Silicon energy bands

[1] D1 and D2: It has been argued that they originate in electronic transition at the geometrical kinks on dislocations [5], point defects [3] and impurities [6] and/or from the reaction products of dislocations [7].

[2] D3 and D4 lines is generally thought to be related to electronic transition within dislocation cores [8]. In addition, it has been suggested that the D3 line most likely is a phonon-assisted replica of D4 [8].

B Sample types and procedures

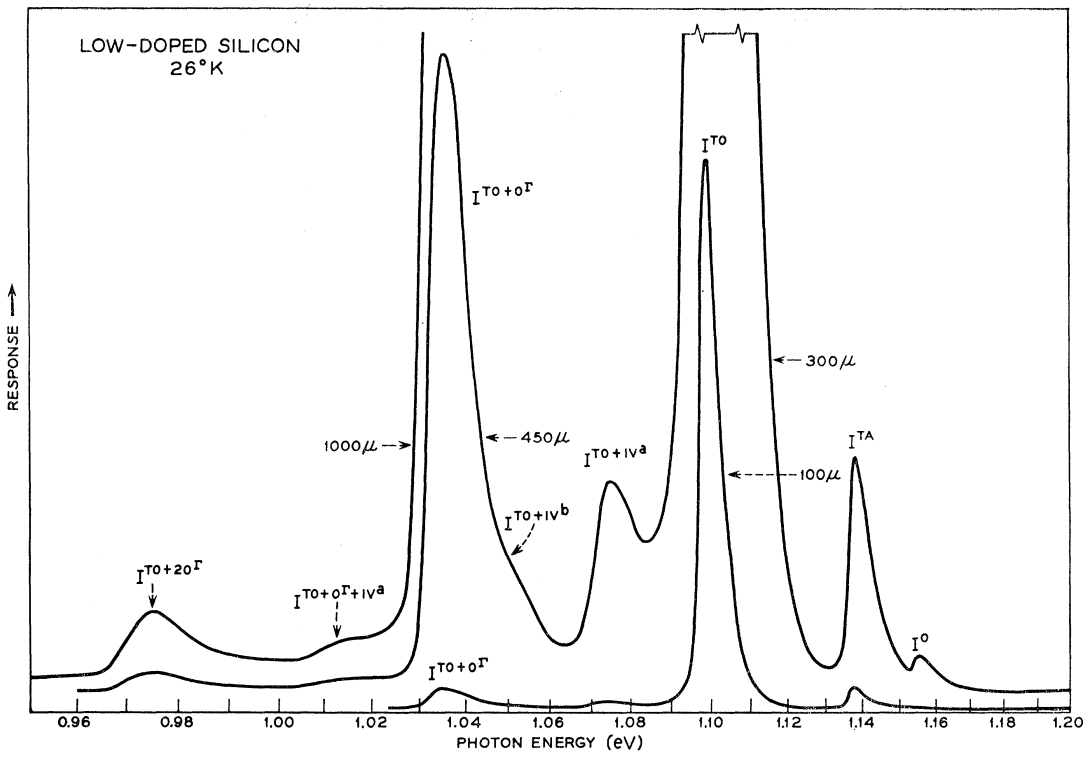

Figure 3: Intrinsic/low doped ($2 \cdot 10^{14} cm^{-3}$ P atoms) Si PL specter from [12]

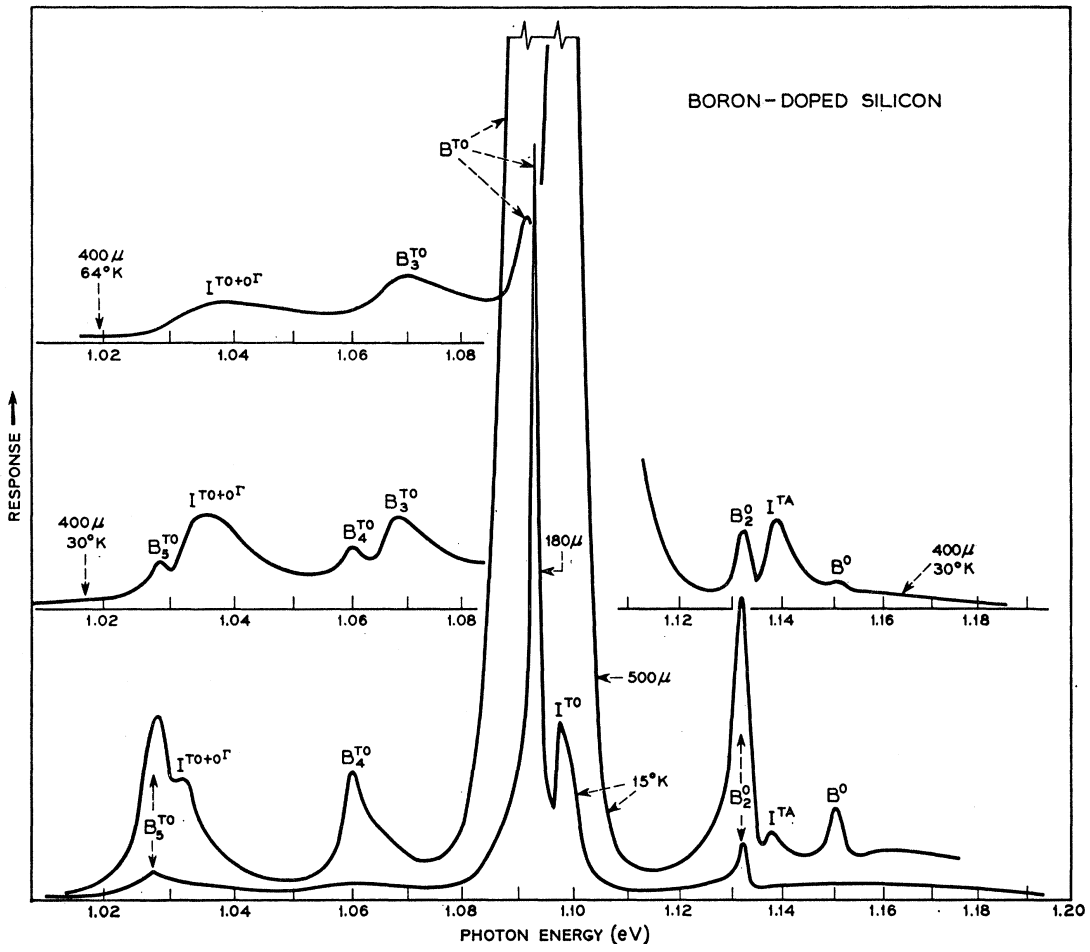

Figure 4: Boron doped ($6 \cdot 10^{16} cm^{-3}$) Si PL specter from [12]

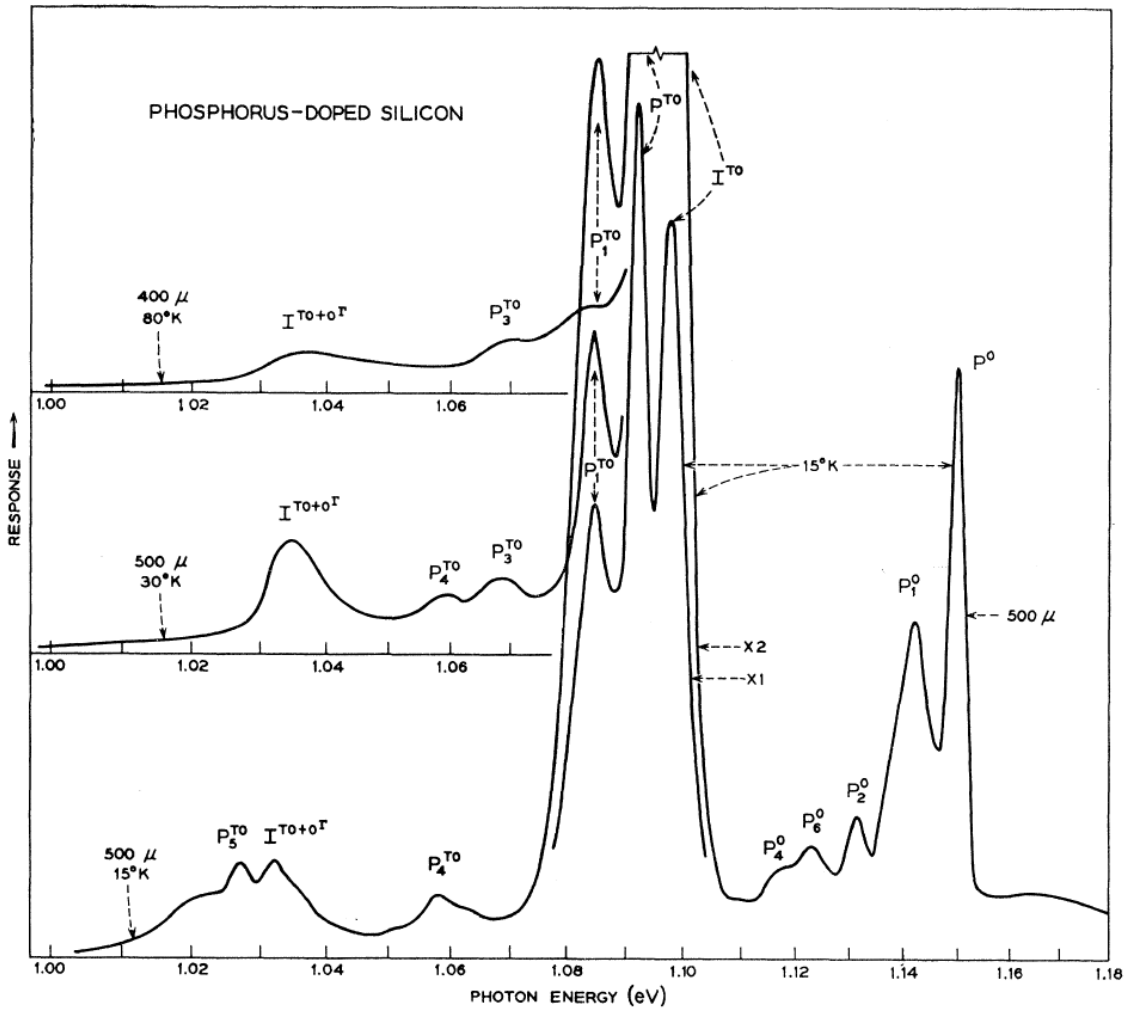

Figure 5: Phosphorus doped ($8 \cdot 10^{16} cm^{-3}$) Si PL specter from [12]

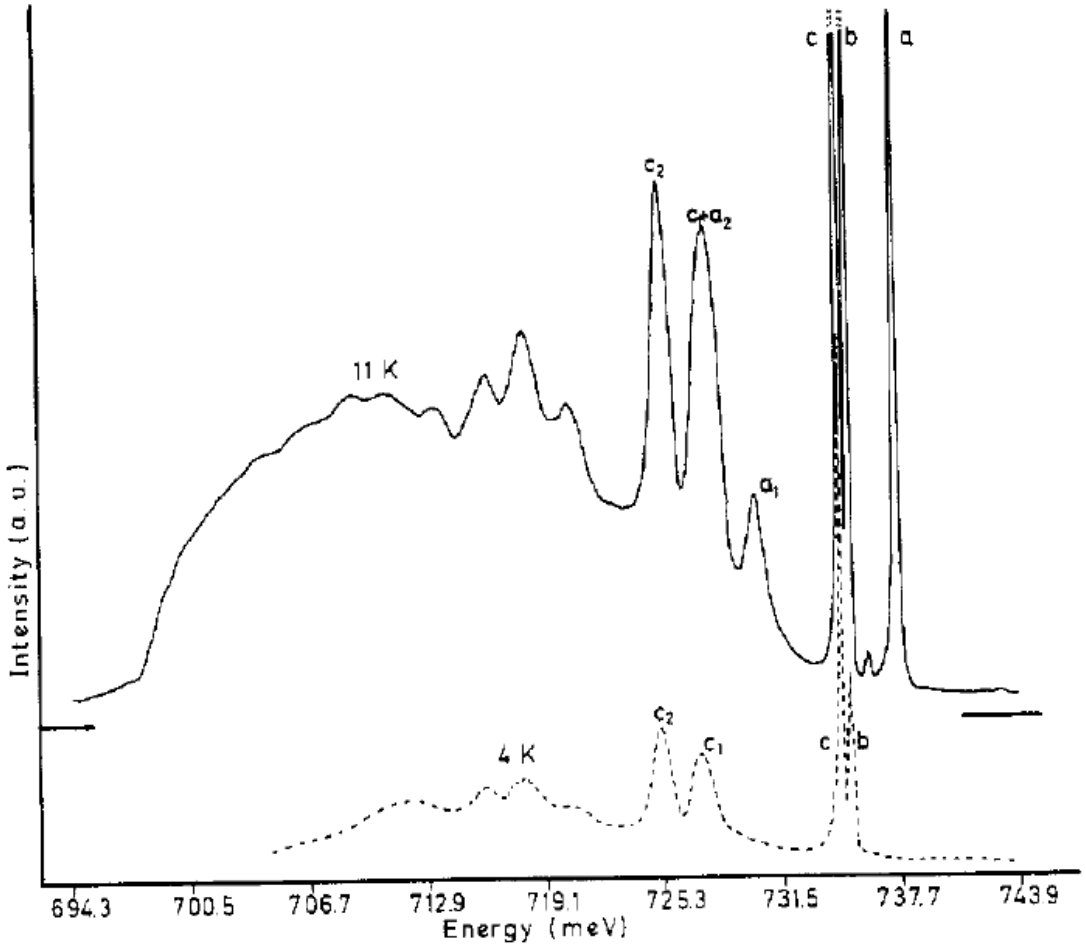

Figure 6: Iron diffused Si sample at two different temperatures from [22]

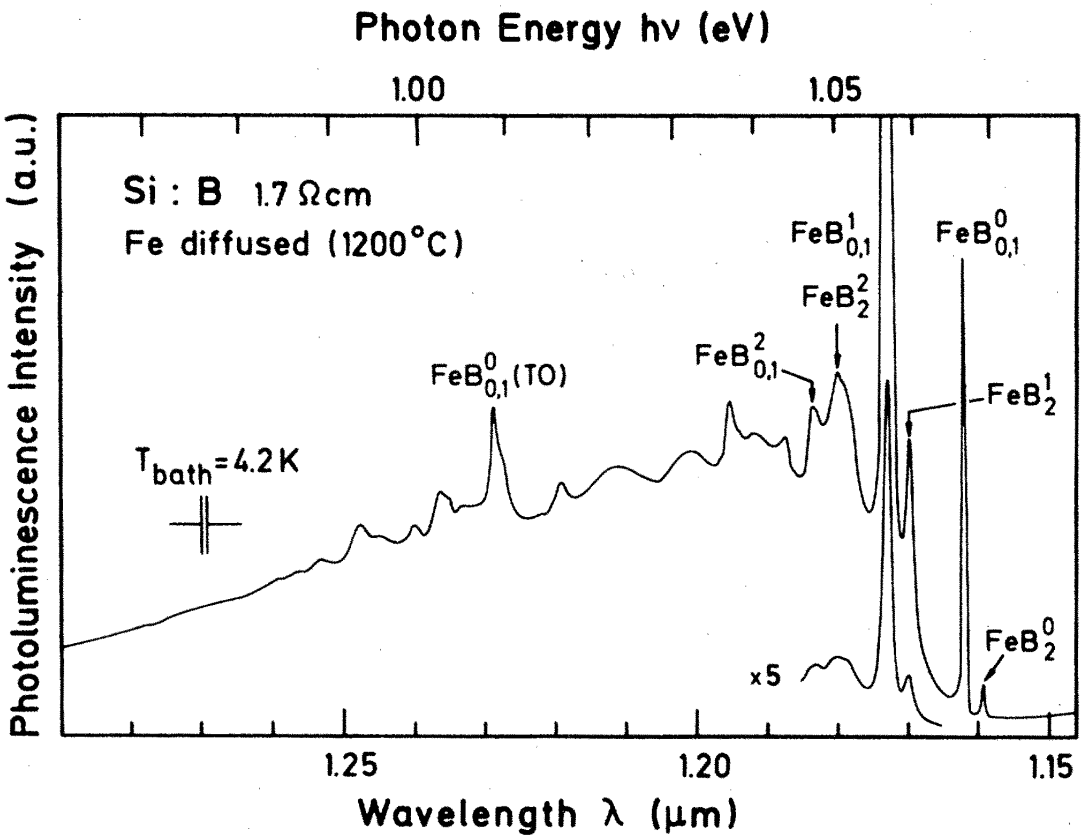

Figure 7: Iron diffused boron doped Si sample from [23]

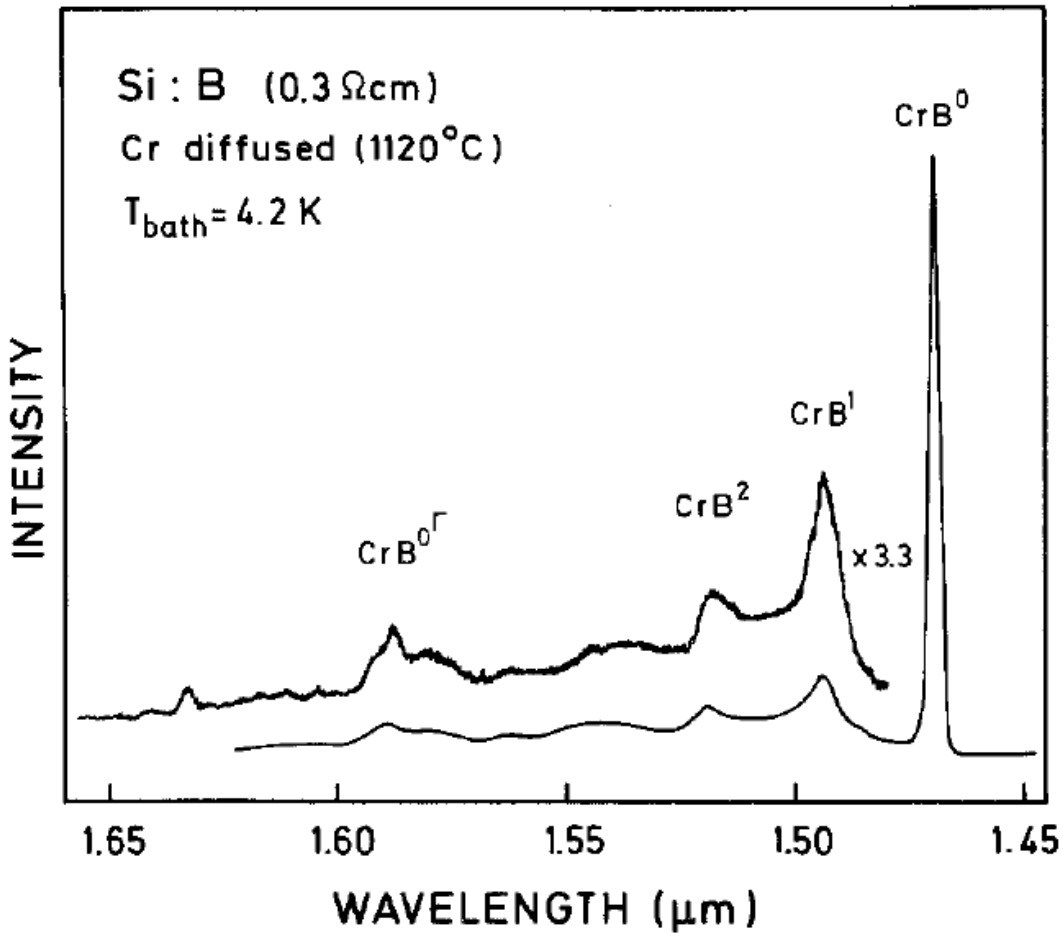

Figure 8: Chromium diffused Boron doped Si sample from [18]

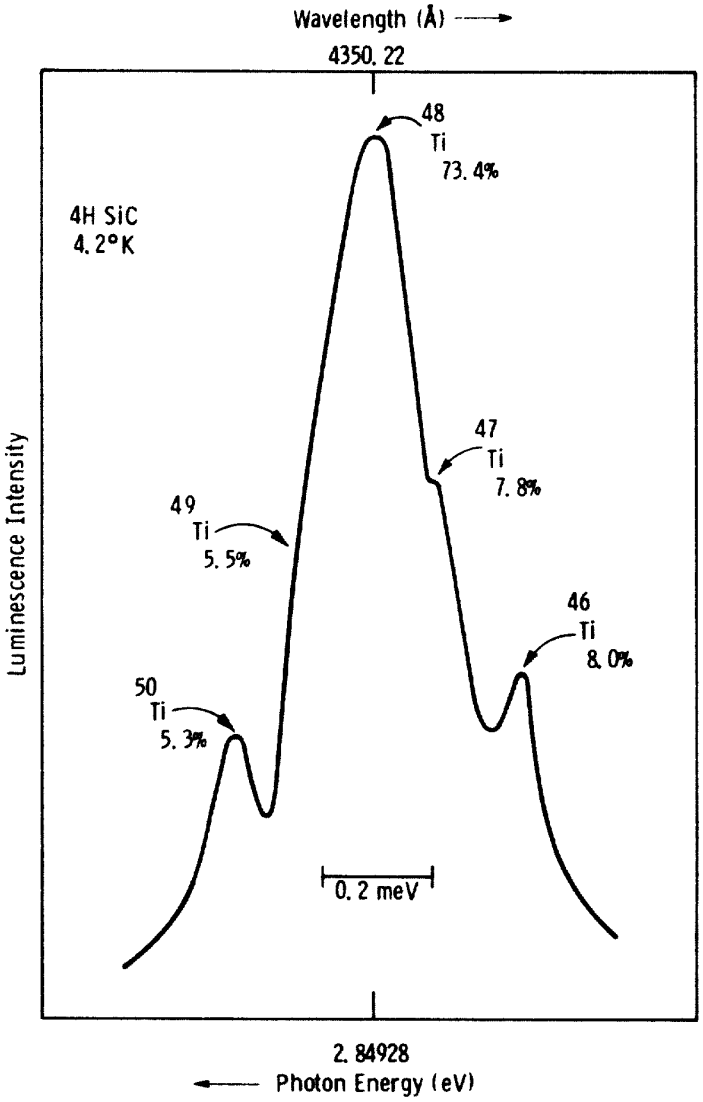

Figure 9: Titanium PL from Ti contaminated 4H SiC

Ref.	Sample type	Excitation process	Area	Processing	Doping
[14]	mc-Si	532nm Nd:YVO_4	$0.1mW/10\ \mu$m diameter	Sawing damage etched by HNO_3/HF	B-doped
[33]	Cz-Si	Kr ion laser 647nm	10 μm		Undoped
[1]	Cz-Si	Xenon lamp	50mW on 3mm modulated at 9Hz	deformed by bending at 850° C	undoped, weak n and p
[10]	mc-Si	800nm AlGaAs laser	Pulsed 300mW / 3mm		Block-casting technique for Baysix
[13]	mc-Si	800nm AlGaAs at 140mW		Produced by EFG	
[50]	mc-Si and FZ-Si	Ar ion 514nm at 300mW	100μm	Produced by EFG	boron doped 10^15cm^-1
[3]	FZ-Si	Kr-ion 647nm, Ar-ion 415nm and Nd-YAG 1064nm		Deformed a 650° C and 850° C	residual 10^{12}cm^{-3} boron
[34]	mc-Si	Nd:YVO 532nm	6mW, 10μm diameter	Slicing damage etched off by HNO_3/HF	boron doped
[18]	FZ-Si and CZ-Si		50mW laser	Etched with HNO_3/HF. Chromium diffused	boron doped
[23]	FZ-Si	Ar+ 514nm	500mW	Fe diffused	boron doped
[22]	FZ-Si	Argon laser		Fe diffusion	undoped
[21]		Ar^+ 514nm at 1.5W			Cu doped
[9]	FZ-Si	Ar^+ 514nm		Heated above a Bunsen burner	Doped with Cu and/or Fe
[51]	mc-Si		6W/cm^2	Polished by HNO_3/HF	Undoped
[12]	CZ-Si	200W mercury arc 2.5eV			Undoped and doped
[30]		Ar^+ or Kr^+ laser 0.6W	0.8mm diameter	Dislocations by bending at 700°C	phosphorus doped

Table 6: Sample types and procedures

C Abbrevations

Abbrevation	Description
B_{TO}	TO phonon replica of the Boron bound exiton
BE	Bound exciton
D_a	Broad background emission
D_b	Oxygen impurity band
CZ-Si	Czochralski processed Silicon
D1	Dislocation related line 1
D1'	Dislocation related line 1 for mc-Si
D2	Dislocation related line 2
D2'	Dislocation related line 2 for mc-Si
D3	Dislocation related line 3
D3'	Dislocation related line 3 for mc-Si
D4	Dislocation related line 4
D4'	Dislocation related line 4 for mc-Si
EBIC	Electron beam induced current
EBSP	Electron Backscatter Diffraction Pattern
EHD	Electron Hole Droplet
FE	Free exciton
FZ-Si	Float-zone silicon
EFG	Edge-define Film-fed Growth
mc-Si	Multicrystalline silicon
R1BB	One phonon replica of band edge emission
R2BB	Two phonon replica of band edge emission
SA GB	Small Angle Grain Boundary
ZPL	Zero Phonon Line

Table 7: Abbreviations